Frequency-Domain Model Order Reduction of Electromagnetic Field in Induction Motor

Toru Shimonishi[1], Takeshi Mifune[1], and Tetsuji Matsuo[1]

[1]Graduate School of Engineering, Kyoto University, Kyoto 615-8510, Japan

A model order reduction method for an induction motor using a Cauer ladder network is developed in the frequency domain. A multiport frequency transformation between the stator and mover domains is derived by neglecting the spatial harmonic interactions. Even after neglecting the harmonic interactions, the reduced model provides a reasonably accurate frequency response, which is more accurate than that of the conventional approximated equivalent circuit.

Index Terms—**Cauer ladder network, induction motor, model order reduction, spatial harmonics**

I. INTRODUCTION

IN recent years, the need for an efficient analysis of motor drive systems has led to the research on model order reduction (MOR) of motors to avoid time-consuming finite element analyses. Based on a magnetostatic approach, the MOR of synchronous motors has been realized [1], [2]. The MOR of induction motors [3]–[5] is under development to cover a wide range of operational conditions. The Cauer ladder network (CLN) method [6] is an efficient and convenient MOR method. Its multiport version has been applied to the MOR of a linear induction motor [3], where the stator and mover domains are separately reduced and connected through spatial harmonic components at the air gap in the time domain to accurately reproduce time-dependent field variables.

Even though the frequency domain analysis is an efficient tool to evaluate steady-state motor properties, the application of the CLN-based MOR [3], [5] to the frequency domain analysis of induction motors was difficult because the spatial harmonics from the slot structure are converted to temporal harmonics. Accordingly, even a sinusoidal current/voltage input yields a distorted voltage/current waveform, which prevents a characteristic analysis under a single frequency condition.

The generation of multiple harmonics results from the interactions between spatial harmonic components, which are represented by the off-diagonal elements of the multiport impedance/admittance matrices in the CLN. Based on this knowledge, this study discusses the frequency transformation between the stator and mover domains to derive the MOR of an induction motor in the frequency domain to evaluate the motor property efficiently without transient computation.

II. MULTIPORT CLN METHOD

A. Multiport CLN method

The eddy-current field in the finite element space is

$$C^{\mathrm{T}}\nu C a = \sigma e + j_0 \ , \quad Ce = -\mathrm{j}\omega C a \qquad (1)$$

where a is the variable vector of vector potential, e is the variable vector of electric field, j_0 is the imposed current, σ is the conductivity matrix, ν is the reluctivity matrix, C is the edge-face incident matrix, and $C^{\mathrm{T}}\nu C$ is the stiffness matrix for the finite element eddy-current analysis.

Let M be the number of ports in the reduced model. The multiport CLN method [3] recursively constitutes the matrices a_{2n-1} and e_{2n} that compose the basis vectors of the vector potential and the electric field, respectively. They are represented as

$$a_{2n-1} = (a_{1,2n-1}, \dots, a_{M,2n-1})$$
$$e_{2n} = (e_{1,2n}, \dots, e_{M,2n}). \qquad (2)$$

The multiport CLN method generates a_{2n-1} and e_{2n} by sequentially solving (3) and (4):

$$C^{\mathrm{T}}\nu C(a_{2n+1} - a_{2n-1}) = \sigma e_{2n} R_{2n} \qquad (3)$$

$$e_{2n+2} - e_{2n} = -a_{2n+1} L_{2n+1}^{-1} \qquad , \qquad (4)$$

where L_{2n-1} and R_{2n} are the inductance and resistance matrices of size $M \times M$. They are given by

$$L_{2n-1} = \{L_{2n-1,l,m}\},$$
$$L_{2n-1,l,m} = a_{l,2n-1}^{\mathrm{T}} C^{\mathrm{T}}\nu C a_{m,2n-1} \qquad (5)$$

$$R_{2n}^{-1} = \{G_{2n,l,m}\},$$
$$G_{2n,l,m} = e_{l,2n}^{\mathrm{T}} \sigma e_{m,2n}. \qquad (6)$$

The electromagnetic fields are expanded using the basis vectors obtained above as

$$a = \sum_n a_{2n-1} I_{2n-1}, \quad e = \sum_n e_{2n} V_{2n} \ . \qquad (7)$$

Here, I_{2n-1} and V_{2n} are coefficient vectors, which are determined by the matrix Cauer network in Fig. 1.

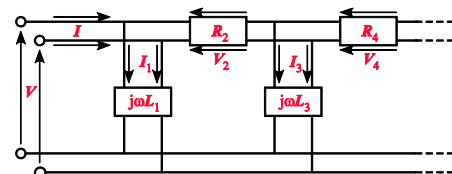Fig. 1. Matrix Cauer network when $M = 2$.

A Self-archived copy in
Kyoto University Research Information Repository
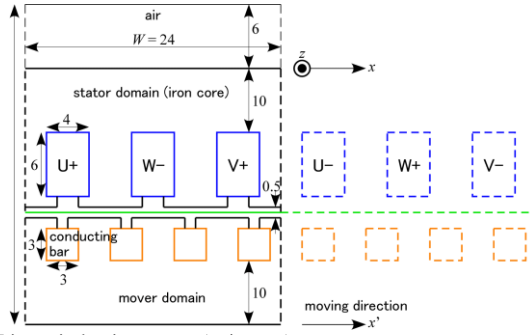https://repository.kulib.kyoto-u.ac.jp

PA-A1-3
2

Fig. 2. Linear induction motor (unit: mm).

When the number of Cauer ladder stages is N, the construction of CLN roughly costs NM times as much as the solution of (1) in the finite element analysis. The nonlinear analysis is realized by parametrizing the inductance and resistance matrices depending on the degree of saturation [7].

B. Spatial harmonic decomposition

The three-phase linear induction motor in Fig. 2 [3] is analyzed; the stator domain is separated from the mover domain at the air gap. For simplicity, the motor length is supposed to be long enough so that the spatially periodic boundary condition can be applied. The multiport CLN method is applied to the stator and mover domains independently with the magnetic field and electric field at the air-gap interface as the input and output, respectively.

(x, y, t) and (x', y', t') are the coordinates of the stator and mover domains, respectively, where

$$x' = x - vt, y' = y, t' = t . \qquad (8)$$

The mover moves in the x-direction at a velocity of v. The two domains are connected by an electric field E_z and a magnetic field H_x at the air-gap interface. Using the time-dependent terms $e^{j\omega t}$ and $e^{j\omega t'}$ in the stator and mover domains, respectively, the magnetic fields H_x and H'_x of the stator and mover domains, respectively, are decomposed as follows:

$$H_x(x,t) = \sqrt{2}\sum_m [H_{cm}\cos(mkx) + H_{sm}\sin(mkx)]e^{j\omega t}$$
$$H'_x(x',t') = \sqrt{2}\sum_m [H'_{cm}\cos(mkx') + H'_{sm}\sin(mkx')]e^{j\omega t'}$$
$$(9)$$

where $k = \pi/W$ is the wave number, and W is half the spatial period. Assuming antiperiodic boundary condition for half-spatial period, the coefficient vectors are represented only with odd harmonic components as:

$$\boldsymbol{I} = [H_{c1}, H_{s1}, H_{c3}, H_{s3}, \cdots],$$
$$\boldsymbol{I}' = [H'_{c1}, H'_{s1}, H'_{c3}, H'_{s3}, \cdots] \qquad (10)$$

Similarly, the electric fields at the interface are represented by the coefficient vectors as

$$\boldsymbol{V} = W[E_{c1}, E_{s1}, E_{c3}, E_{s3}, \cdots],$$
$$\boldsymbol{V}' = W[E'_{c1}, E'_{s1}, E'_{c3}, E'_{s3}, \cdots] \qquad (11)$$

$$\boldsymbol{\Phi} = W[A_{c1}, A_{s1}, A_{c3}, A_{s3}, \cdots],$$
$$\boldsymbol{\Phi}' = W[A'_{c1}, A'_{s1}, A'_{c3}, A'_{s3}, \cdots] \qquad (12)$$

where

$$\boldsymbol{V} = -j\omega\boldsymbol{\Phi} \ , \ \boldsymbol{V}' = -j\omega'\boldsymbol{\Phi}' . \qquad (13)$$

C. Matrix Cauer form representation

The three-phase source current and voltage are defined as
$$\boldsymbol{I}_0 = [I_U, I_V, I_W], \boldsymbol{V}_0 = [V_U, V_V, V_W]. \qquad (14)$$

In this study, the iron loss is neglected for simplicity, even though it can be considered by homogenization [3]. In this case, the input to the multiport CLN for the stator is $(\boldsymbol{I}_0, \boldsymbol{I})$, which is related to the output $(\boldsymbol{V}_0, \boldsymbol{V})$ as:

$$\boldsymbol{V}_0 = \boldsymbol{Z}_{00}\boldsymbol{I}_0 + \boldsymbol{Z}_{01}\boldsymbol{I}$$
$$\boldsymbol{V} = \boldsymbol{Z}_{10}\boldsymbol{I}_0 + \boldsymbol{Z}_{11}\boldsymbol{I} . \qquad (15)$$

The relation in the mover domain is represented as

$$\boldsymbol{V}' = \boldsymbol{Z}'\boldsymbol{I}' \qquad (16)$$

where $\boldsymbol{Z}'$ is the impedance matrix in the mover domain. These variables are used in both the frequency and time domains for simplicity of notation. The multiport transfer functions above are given in matrix continued fraction forms, meaning they are represented by matrix Cauer forms, as shown in Fig. 1.

D. Representation in frequency domain

The interface magnetic fields H_x and H'_x are rewritten using the forward and backward wave components as

$$H_x = \sqrt{2}\sum_m (H_{fm}e^{-jmkx} + H_{bm}e^{jmkx})e^{j\omega t}$$
$$H'_x = \sqrt{2}\sum_m (H'_{fm}e^{-jmkx'} + H'_{bm}e^{jmkx'})e^{j\omega t'} . \qquad (17)$$

Using (8), the components of H_x are rewritten as

$$(H_{fm}e^{-jmkx} + H_{bm}e^{jmkx})e^{j\omega t}$$
$$= H_{fm}e^{-jmkx'}e^{j\omega[1-m(1-s)]t'} + H_{bm}e^{jmkx'}e^{j\omega[1+m(1-s)]t'} \qquad (18)$$

where s is the slip that is defined from the moving speed v as

$$v = (1-s)\frac{\omega}{k}. \qquad (19)$$

From (17), (18) and the boundary condition $H_x = H_x'$, the boundary condition of the forward and backward wave components at the gap interface are given as

$$H_{fm}(j\omega) = H'_{fm}(j\omega[1-m(1-s)]) = H'_{fm}(j\omega'_{fm})$$
$$H_{bm}(j\omega) = H'_{bm}(j\omega[1+m(1-s)]) = H'_{bm}(j\omega'_{bm}) \qquad (20)$$

where ω'_{fm} and ω'_{bm} are the angular frequencies of the forward and backward waves, respectively, depending on s. They are defined as

$$s_{fm} = 1 - m(1-s), s_{bm} = 1 + m(1-s)$$
$$\omega'_{fm} = s_{fm}\omega, \omega'_{bm} = s_{bm}\omega \qquad (21)$$

where s_{fm} and s_{bm} are the slips of the forward and backward waves, respectively. Similarly, the boundary condition for the vector potential is given as

$$A_{fm}(j\omega) = A'_{fm}(j\omega'_{fm}) \ , \ A_{bm}(j\omega) = A'_{bm}(j\omega'_{bm}). \qquad (22)$$

Using the vector potential, the electric field is given as

京都大学
KYOTO UNIVERSITY
PA-A1-3

A Self-archived copy in
Kyoto University Research Information Repository
https://repository.kulib.kyoto-u.ac.jp

京都大学学術情報リポジトリ
KURENAI 紅
Kyoto University Research Information Repository

3

$$E_{fm} = -j\omega A_{fm}, \; E_{bm} = -j\omega A_{bm},$$
$$E'_{fm} = -j\omega'_{fm}A'_{fm}, \; E'_{bm} = -j\omega'_{bm}A'_{bm}. \tag{23}$$

Consequently, the boundary condition for the electric field is given as

$$E'_{fm}(j\omega'_{fm}) = s_{fm}E_{fm}(j\omega),$$
$$E'_{bm}(j\omega'_{bm}) = s_{bm}E_{bm}(j\omega). \tag{24}$$

The forward and backward wave components of the magnetic and electric fields are represented by coefficient vectors as

$$H = [H_{f1}, H_{b1}, H_{f3}, H_{b3}, \ldots],$$
$$H' = [H'_{f1}, H'_{b1}, H'_{f3}, H'_{b3}, \ldots] \tag{25}$$

$$E = W [E_{f1}, E_{b1}, E_{f3}, E_{b3}, \ldots],$$
$$E' = W [E'_{f1}, E'_{b1}, E'_{f3}, E'_{b3}, \ldots]. \tag{26}$$

The comparison of (17) with (9) gives the relationships between the cos/sin components and the forward and backward wave components as:

$$E = QV, \; H = QI$$
$$E' = QV', \; H' = QI' \tag{27}$$

where Q is the transformation matrix given as

$$Q = \text{blockdiag}[P, P, \ldots] \tag{28}$$

$$P = \begin{bmatrix} 1/2 & j/2 \\ 1/2 & -j/2 \end{bmatrix}, P^{-1} = \begin{bmatrix} 1 & 1 \\ -j & j \end{bmatrix}. \tag{29}$$

The slip matrix s is defined as

$$s = \text{diag}[s_{f1}, s_{b1}, s_{f3}, s_{b3}, \ldots]. \tag{30}$$

Using s, (24) can be written as

$$E' = sE, \tag{31}$$

whereas the boundary conditions of the magnetic field are given as

$$H' = H. \tag{32}$$

E. Derivation of motor impedance matrices

Equation (16) represents the relation for the sin/cos components on the mover side, which are converted to the relation for forward/backward wave components as

$$E' = QZ'Q^{-1}H' = \underline{Z}'H',$$
$$\underline{Z}' = QZ'Q^{-1} \tag{33}$$

where $\underline{Z}'$ is the impedance matrix for the forward/backward wave components on the mover side. Note that $\underline{Z}'$ depends on the slip frequencies ($s_{fm}\omega$ or $s_{bm}\omega$), which are functions of the harmonic order m. In the moving coordinate, the angular frequency depends on the harmonic order m, where the backward wave has a different angular frequency from that of the forward wave.

From (31), (32), and (33), the relation for the forward/backward components on the stator side is given as:

$$E = s^{-1}\underline{Z}'H' = \underline{Z}''H,$$
$$\underline{Z}'' = s^{-1}\underline{Z}' = s^{-1}QZ'Q^{-1} \tag{34}$$

where $\underline{Z}''$ is the impedance matrix for the forward/backward

wave components on the stator side. The relation for the sin/cos components on the stator side is given as

$$V = Q^{-1}\underline{Z}''QI = Z''I,$$
$$Z'' = Q^{-1}\underline{Z}''Q \tag{35}$$

where Z'' is the impedance matrix of the sin/cos components in the stator.

Using (15) and (35), the magnetic field I at the gap interface is given by

$$I = (Z'' - Z_{11})^{-1} Z_{10}I_0. \tag{36}$$

The motor impedance matrix Z_0 is defined from $V_0 = Z_0I_0$, which is obtained by eliminating I from (15) and (36) as follows:

$$Z_0 = Z_{00} + Z_{01}(Z'' - Z_{11})^{-1}Z_{10}. \tag{37}$$

The air-gap power P_2 transferred to the mover domain is given by $P_2 = \text{Re}(-V^TI^*)$, where * denotes the complex conjugate. The thrust force $F_x = \int_0^W H_x B_y dx$ at the air gap is obtained as follows [3]:

$$F_x = \text{Re}(B^TI^*), \tag{38}$$

where B is given as

$$B = kW [-A_{s1}, A_{c1}, -3A_{s3}, 3A_{c3}, \ldots]. \tag{39}$$

A factor of $1/2$ is used by P_2 and F_x above if the coefficients are not effective values, but temporal amplitudes.

F. Approximation of spatial harmonic interactions

The spatial harmonic components are not independent but interact with each other. For example, even if I' has only the l-th spatial harmonic component on the mover side, V' given in (16) has the l'-th component unless the (l', l)-element of Z' is 0. The l'-th component of V' is converted to V in the stator domain with a different temporal frequency because of the frequency transformation (21). Accordingly, frequency domain analysis becomes difficult because the interaction converts the slot harmonics into temporal harmonics due to the slot structure. Accordingly, even a sinusoidal current/voltage input yields temporal harmonics of the voltage/current waveform, which prevents motor analysis under a single frequency condition.

Similarly to Z', the interactions among the spatial harmonic components are represented by the off-diagonal elements of the multiport impedance/admittance matrices in the CLN. To realize the frequency domain analysis, the spatial harmonic interaction is neglected in the mover-domain CLN, as follows:

[Method A]–The off-diagonal components of the mover network element matrices are ignored after constructing them using the multiport CLN method.

[Method B]–Each diagonal component of Z' is independently computed by the single-port CLN method without considering the other harmonic components. To compute only the diagonal elements, (5) and (6) are modified.

$$L'_{2n-1} = \text{diag}(L'_{2n-1,1,1l}, L'_{2n-1,3,3}, \ldots),$$
$$L'_{2n-1,l,l} = a_{l,2n-1}^T C^T v C a_{l,2n-1}, \tag{40}$$

$$\boldsymbol{R}_{2n}^{\prime-1} = \mathrm{diag}(G_{2n,1,1}^{\prime}, G_{2n,3,3}^{\prime}, \dots),$$
$$G_{2n,l,l}^{\prime} = \boldsymbol{e}_{l,2n}^{\mathrm{T}} \boldsymbol{\sigma} \boldsymbol{e}_{l,2n}. \tag{41}$$

The process of the multiport CLN method using method B is equivalent to performing a single-port CLN M times.

The approximations above neglect the generation of additional temporal harmonics assuming that their contribution to the average motor characteristics is small.

III. NUMERICAL ANALYSIS

A sinusoidal three-phase current $\boldsymbol{I}_0$ with an amplitude of 1 AT is fed to the linear induction motor [Fig. 2]. The resistance of the stator windings is not included in the stator-side CLN; however, it can be inserted between the power source and stator-side CLN. The relative permeability of the iron core is 1000 and the conductivity of the mover bar is 3×10^7 S/m. Fig. 3 shows the frequency dependence of the inductance observed from one phase of the three-phase ports when the 1st to 11th spatial harmonic components are considered. The slip is set to 0.1. There are four stages of the Cauer circuit in the mover domain. Method B provides a result closer to that of the finite element analysis in the high-frequency range than method A.

Fig. 4 shows the speed dependence of the thrust force F_x and gap power given by method B at 50 Hz, where the 1st to $(2K-1)$th spatial harmonics are included with $K = 1$, 4, and 6. The accuracy is improved by including higher spatial harmonics. It seems reasonable to choose $2K-1$ a little larger than the numbers of stator slots and mover bars per pole-pair for accurate analysis.

Next, the frequency-domain analysis using method B was compared with the analysis using the conventional approximate equivalent circuit [8]. Fig. 5 shows the speed dependence of F_x at 50 Hz, where the mean square errors compared with the finite element analysis are indicated in parentheses ("er."). The approximate equivalent circuit is less accurate than the CLN method in the frequency domain with the 1st to 11th spatial harmonics.
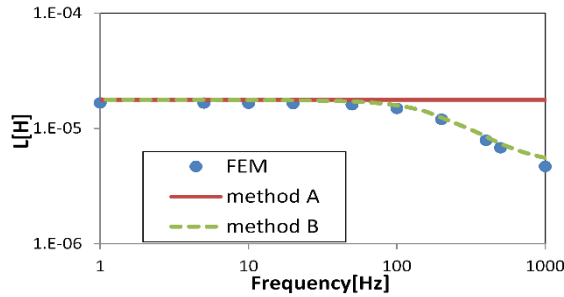

Fig. 3. Frequency dependence of inductance.

IV. CONCLUSION

The MOR of the induction motor in the frequency domain was realized by neglecting the interaction between the spatial harmonic components at the gap interface. Because the spatial harmonics are multiple inputs in the multiport CLN method, neglecting the spatial harmonic interaction results in the single-port CLN method. The proposed frequency-domain method provides reasonably accurate properties of the induction motor, which are more accurate than the conventional equivalent circuit.

REFERENCES

[1] T. Henneron, S. Clénet, "Model order reduction applied to thenumerical study of electrical motor based on POD method taking into account rotation movement," *Int. J. Numer. Model.*, vol. 27, pp.485-494, 2014.

[2] T. Shimotani, Y. Sato, T. Sato, and H. Igarashi, "Fast finite-element analysis of motors using block model order reduction," *IEEE Trans. Magn.*, vol. 52, 7207004, Mar. 2016.

[3] T. Matsuo, K. Sugahara, A. Kameari and Y. Shindo, "Model order reduction of an induction motor using a Cauer ladder network," *IEEE Trans. Magn.*, vol. 56, 7514704, Mar. 2020.

[4] L. Montier, T. Henneron, S. Clénet, and B. Goursaud, "Model order reduction applied to a linear finite element model of a squirrel cage induction machine based on POD approach," *IEEE Trans. Magn.*, vol. 57, 3066678, Jun. 2021.

[5] Y. Takahashi, K. Fujiwra, K. Sugahara, and T. Matsuo "Reduced order modeling based on multiport Cauer ladder network for space harmonics of air-gap flux density in cage induction motor," *IEEE Trans. Magn.*, (early access).

[6] A. Kameari, H. Ebrahimi, K. Sugahara, Y. Shindo and T. Matsuo, "Cauer ladder network representation of eddy-current fields for model order reduction using finite element method," *IEEE Trans. Magn.*, vol. 54, 7201804, Mar. 2018.

[7] M. Tobita and T. Matsuo, "Nonlinear model order reduction of induction motors using parameterized CLN method," *IEEE Trans. Magn.* (to appear).

[8] K.R. Siddhapura and D.B. Raval, *A Textbook of Electrical Machines*, Vikas Publishing House, 2014.
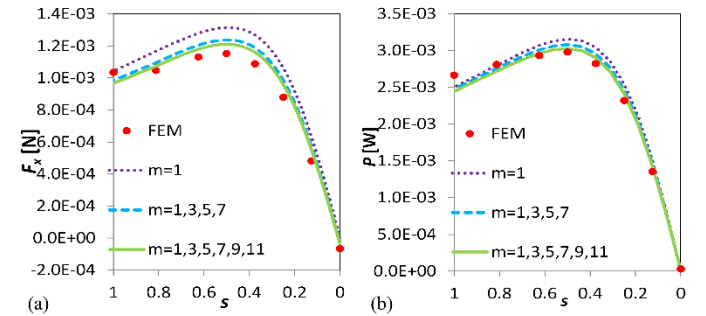
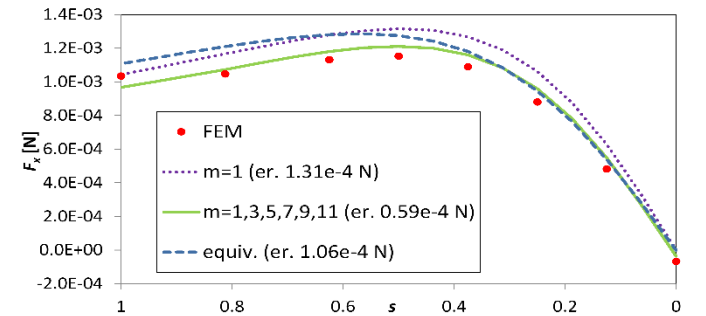Fig. 4. Speed dependence of (a) thrust force and (b) gap power.

Fig. 5. Speed dependence of thrust force given by conventional approximate equivalent circuit of L-type ("equiv" in the figure); "er." indicates mean square error compared with FEM.